American Journal of Optics and Photonics
2015; 3(6): 123-128
Published online December 21, 2015 (http://www.sciencepublishinggroup.com/j/ajop)
doi: 10.11648/j.ajop.20150306.11
ISSN: 2330-8486 (Print); ISSN: 2330-8494 (Online)

The Potential Impact of Biofield Energy Treatment on the Atomic and Physical Properties of Antimony Tin Oxide Nanopowder

Mahendra Kumar Trivedi[1], Rama Mohan Tallapragada[1], Alice Branton[1], Dahryn Trivedi[1], Gopal Nayak[1], Omprakash Latiyal[2], Snehasis Jana[2, *]

[1]Trivedi Global Inc., Henderson, USA
[2]Trivedi Science Research Laboratory Pvt. Ltd., Bhopal, Madhya Pradesh, India

Email address:
publication@trivedisrl.com (S. Jana)

To cite this article:
Mahendra Kumar Trivedi, Rama Mohan Tallapragada, Alice Branton, Dahryn Trivedi, Gopal Nayak, Omprakash Latiyal, Snehasis Jana. The Potential Impact of Biofield Energy Treatment on the Atomic and Physical Properties of Antimony Tin Oxide Nanopowder. *American Journal of Optics and Photonics.* Vol. 3, No. 6, 2015, pp. 123-128. doi: 10.11648/j.ajop.20150306.11

Abstract: Antimony tin oxide (ATO) is known for its high thermal conductivity, optical transmittance, and wide energy band gap, which makes it a promising material for the display devices, solar cells, and chemical sensor industries. The present study was undertaken to evaluate the effect of biofield energy treatment on the atomic and physical properties of ATO nanopowder. The ATO nanopowder was divided into two parts: control and treated. The treated part was subjected to Mr. Trivedi's biofield energy treatment. The control and treated samples were analyzed using X-ray diffraction (XRD), Fourier transform infrared (FT-IR) spectroscopy, and electron spin resonance (ESR) spectroscopy. The XRD data revealed that the crystallite size on the plane (110) was significantly reduced to 53.1 nm as compared to the control (212.6 nm). In addition, the lattice parameter, unit cell volume, density, and molecular weight were also altered as compared to the control. The FT-IR spectra showed that the stretching vibration corresponding to Sn-OH was shifted to higher wavenumber (512 cm^{-1}) in the treated sample as compared to the control (496 cm^{-1}). Besides, ESR spectral analysis exhibited that the g-factor was reduced in the treated ATO sample by 21.1% as compared to the control. Also, the ESR signal width and height were reduced by 70.4% and 93.7%, respectively as compared to the control. Hence, the XRD, FT-IR, and ESR data revealed that the biofield energy treatment has a significant impact on the atomic and physical properties of ATO nanopowder. Therefore, the biofield energy treatment could be more useful in display devices and solar cell industries.

Keywords: Antimony Tin Oxide, Nanopowder, Biofield Energy Treatment, X-Ray Diffraction, Fourier Transform Infrared, Electron Spin Resonance

1. Introduction

Transparent conducting oxides (TCO) are well known for their wide energy band gap, optical transmittance and electric conductivity [1]. Due to this, TCO are utilized in solar cell, display devices, UV and optical devices [2]. Recently, antimony tin oxide (ATO), an antimony (Sb) doped tin oxide (SnO_2) has gained significant attention due to their applications in transparent conducting electrodes, chemical sensors, and dye sensitized solar cell [3-7]. In ATO, the SnO_2 has a rutile tetragonal crystal structure, where Sn atoms are situated at the corner and oxygen is occupying the tetrahedral interstitial sites [8]. Furthermore, Sb dopants occupy the Sn sites in the rutile structure that has been extensively studied by using Extended X-Ray Absorption Fine Structure (EXAFS) [9]. Stjerna *et al.* reported that the increase in Sb concentration led to increase the charge carrier concentration [10]. The presence of Sb modify the band structure of SnO_2 and form a Sb-5s like band in SnO_2 [11]. Besides, for industrial applications the crystal structure properties, bonding properties, and physical properties of ATO plays a crucial role. Currently, these properties are controlled using several processes such as sol–gel [12], co-precipitation [9], combustion route [13], mechanochemical [14], laser ablation [15], and microemulsions [16] techniques. However, these process have certain limitation such as large crystallite size, non-uniformity etc. Thus, it is important to study an approach

i.e. biofield energy treatment, which may be used to modify the physical and atomic properties of ATO nanopowder, when it is produced through conventional methods.

The energy exists in various forms such as thermal, electric, kinetic, nuclear, etc. It is also known that the energy can be transferred from one place to another place using several scientific techniques. Moreover, the living organisms are exchanging their energy with the environment for their health maintenance [17]. Thus, a human has the capability to harness the energy from the environment/Universe and transmit it to any object around the Globe. The object(s) receive the energy and respond in a useful way that is called biofield energy, and this process is known as biofield energy treatment. The National Center for Complementary and Alternative Medicine (NCCAM) has recommended the use of alternative CAM therapies (*e.g.* healing therapy) in the healthcare sector [18]. Beside this, Mr. Trivedi's unique biofield energy treatment (The Trivedi Effect®) had been extensively studied in various scientific fields such as materials science [19,20], microbiology [21], etc. In materials science, biofield energy treatment has significantly altered the atomic, physical, structural, and thermal properties in several metals [22, 23] and ceramics [24]. Thus, after conceiving the effect of biofield energy treatment on metals and ceramics, this study was designed to evaluate the effect of this treatment on the atomic and physical properties of the ATO nanopowder using X-ray diffraction (XRD), Fourier transform infrared (FT-IR) spectroscopy, and electron spin resonance spectroscopy (ESR).

2. Materials and Methods

The ATO nanopowder was obtained from Sigma Aldrich, USA. The nanopowder sample was equally distributed into two parts: control and treated. The control sample was remained as untreated, while the treated sample was in sealed pack, handed over to Mr. Trivedi for biofield energy treatment under standard laboratory condition. Mr. Trivedi provided the treatment through his energy transmission process to the treated sample without touching the sample. After that, the control and treated ATO nanopowder samples were characterized using XRD, FT-IR, and ESR techniques.

2.1. XRD Study

For, XRD study, approximately 500 mg of sample was weighed. The samples were prepared by back loading technique using sample preparation kit. In this process, the sample holder ring was fixed to the sample preparation table and the sample was spread in the holder ring in sufficient quantity to fill the ring cavity. The Phillips, Holland PW 1710 X-ray diffractometer system was used to perform the XRD analysis of control and treated ATO nanopowder samples. The data obtained from the XRD system was in the form of a table, which includes the Bragg angles, the peak intensity counts, relative intensity (%), d-spacing value (Å), and full width half maximum (FWHM) (θ°). After that, the PowderX software was used to calculate the crystal structure parameters such as lattice parameter, and unit cell volume of the control and treated samples. Also, the Scherrer equation was used to compute the crystallite size on various planes as given below:

$$Crystallite\ size\ (G) = \frac{k\lambda}{b\ cos\theta}$$

Here, k is equipment constant (=0.94), λ =1.54056 Å, b is full width half maximum (FWHM). After that the percentage change in G was calculated using following formula:

$$Percent\ change\ in\ crystallite\ size\ (G) = \frac{G_t - G_c}{G_c} \times 100$$

Where, G_c and G_t are the crystallite size of control and treated ATO nanopowder samples respectively.

2.2. FT-IR Spectroscopy

For FT-IR characterization, the samples were crushed into fine powder and mixed in spectroscopic grade KBr in an agate mortar. Then the mixture was pressed into pellets with a hydraulic press. The FT-IR analysis of control and treated ATO nanopowder was performed on Shimadzu's Fourier transform infrared spectrometer (Japan) with frequency range of 4000-500 cm^{-1}. The purpose of the FT-IR analysis was to study the impact of biofield energy treatment on dipole moment, force constant and bond strength in the ATO nanopowder.

2.3. ESR Spectroscopy

The ESR analysis of control and treated ATO nanopowder samples was carried out using Electron Spin Resonance (ESR), E-112 ESR Spectrometer, Varian USA. The X-band microwave frequency (9.5 GHz), with sensitivity of 5 x 1010, ΔH spins was used for the ESR study.

3. Results and Discussion

3.1. XRD Study

The XRD patterns of control and treated ATO samples are shown in Fig. 1. The control ATO sample showed the intensive XRD peaks at Bragg angle 26.55°, 33.89°, 37.97°, and 51.77°, which were indexed to crystalline plane (110), (101), (200), and (211) of tetragonal crystal structure as per joint committee on powder diffraction standards (JCPDS) card no. 21-1252 [25, 26]. Further, the treated sample (T1) showed the crystalline peaks, corresponding to planes (110), (101), (200), and (211) at lower Bragg's angle as 26.49°, 33.86°, 37.93°, and 51.75° respectively, as compared to the control. However, the treated sample T2 showed that the crystalline peak corresponding to the plane (110) was shifted to higher Bragg angle as 26.58° as compared to the control (26.55°). Contrarily, the crystalline peak corresponding to plane (101) was shifted to lower Bragg angle as 33.79° in T2 as compared to the control (33.89°). Thus, the shifting of the crystalline peaks of ATO after biofield energy treatment

suggested the presence of internal strain in the treated ATO samples. It was reported that the increase in lattice parameter of unit cell led to shift the XRD peaks toward lower Bragg angle and *vice versa* [27]. Besides, the crystallite size of control and treated samples on each crystalline plane were computed using Scherer equation and result are presented in Table 1. The data showed that the crystallite size on crystalline plane (110) was significantly reduced in the treated sample T1 (85 nm) and T2 (53.1 nm) as compared to the control (212.6 nm). Also, the crystallite size on plane (211) was altered from 65.7 nm (control) to 76.7 nm and 30.7 nm in T1 and T2 samples, respectively. However, the crystallite sizes on planes (101) and (200) were found same in both control and treated samples. It was reported that the increase in dopant concentration of antimony in tin oxide led to increase the crystallite size and *vice versa* [28]. Zhang et al. reported that the change in crystallite boundaries due to alteration in crystallite size affects the conductivity of ATO [29]. Thus, it is possible that the biofield energy treatment may alter the conductivity of ATO by changing its crystallite boundaries area. Furthermore, the crystal structure parameters of ATO sample were computed using PowderX software and presented in Table 2. It was found that the lattice parameter of tetragonal unit cell was increased from 4.753 Å (control) to 4.757 Å and 4.766Å in T1 and T2, respectively. The increase in lattice parameter in treated samples led to increase the unit cell volume to 7.206×10^{-23} cm^3 and 7.234×10^{-23} cm^3 in T1 and T2, respectively, as compared to the control (7.030×10^{-23} cm^3). Furthermore, the increase in unit cell volume led to reduce the density from 7.030 g/cc (control) to 7.018 g/cc and 6.992 g/cc in T1 and T2 respectively, while the molecular weight was increased from 153.06 g/mol (control) to 153.30 g/mol to 153.89 g/mol in T1 and T2 respectively. Thus, the above results suggested that the biofield energy treatment probably acted at atomic level to cause these modification. It is assumed that the energy transferred through biofield treatment could be in the form of the neutrinos, which probably acted at nuclear level to cause these alterations.

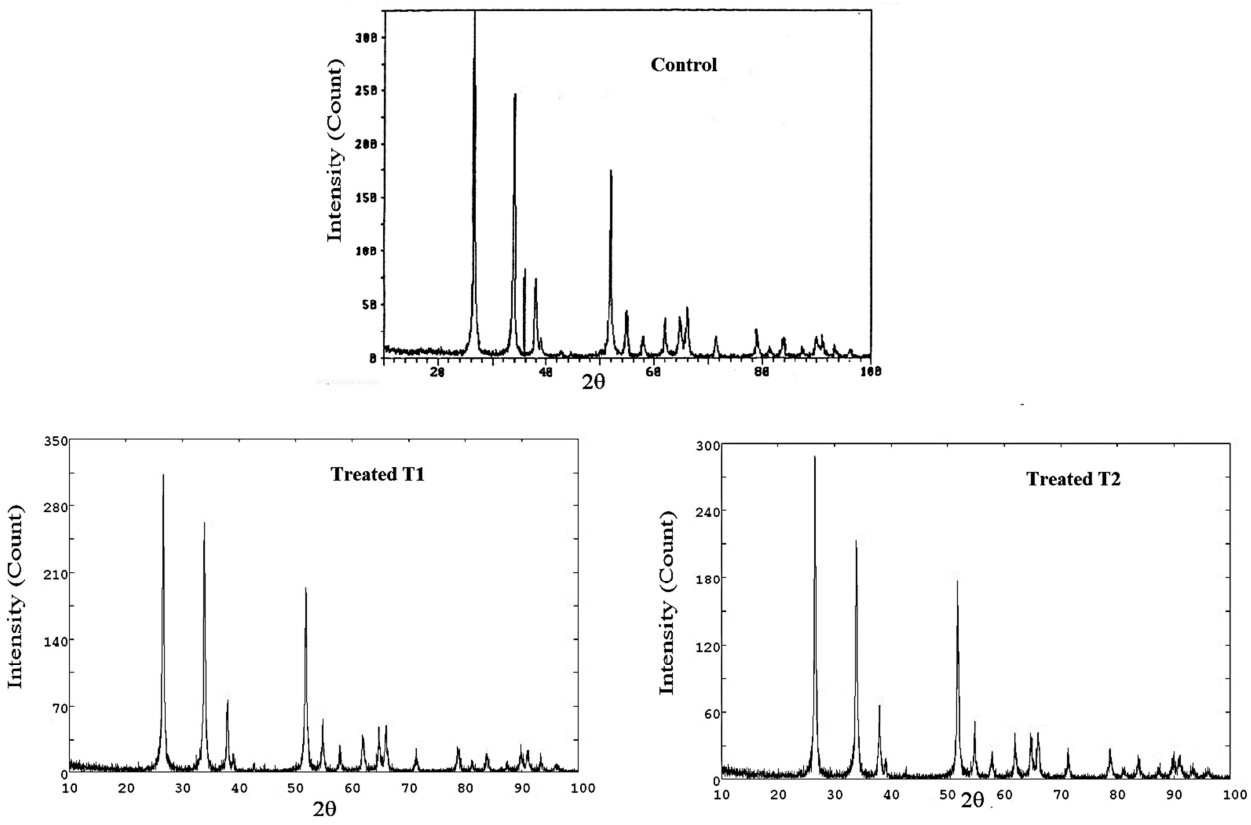

Fig. 1. *X-ray diffractogram of antimony tin oxide nanopowder.*

Table 1. *Effect of biofield energy treatment on crystallite size of antimony tin oxide nanopowder.*

Plane (hkl)	Control			T1			T2		
	2 θ (°)	FWHM (°)	G (nm)	2 θ (°)	FWHM (°)	G (nm)	2 θ (°)	FWHM (°)	G (nm)
110	26.55	0.04	212.6	26.49	0.1	85.0	26.58	0.16	53.1
101	33.89	0.08	108.1	33.86	0.08	108.1	33.79	0.08	108.1
200	37.97	0.18	48.6	37.93	0.18	48.6	37.95	0.18	48.6
211	51.77	0.14	65.7	51.75	0.12	76.7	51.75	0.3	30.7

2 θ is Bragg angle, FWHM is full width half maximum of peaks, and G is crystallite size

Table 2. *Effect of biofield energy treatment on lattice parameter, unit cell volume density atomic weight, nuclear charge per unit volume of antimony tin oxide nanopowder.*

Group	Lattice parameter (Å)	Unit cell volume ($\times 10^{-23}$ cm^3)	Density (g/cc)	Molecular weight (g/mol)
Control	4.7535	7.194	7.030	153.060
T1	4.7573	7.206	7.018	153.303
T2	4.7664	7.234	6.992	153.892

3.2. FT-IR Spectroscopy

The FT-IR spectra of control and treated ATO samples is presented in Figure 2. The spectra showed the absorption bands at 3445 cm^{-1} and 3439 cm^{-1} in control and treated sample, respectively, which was attributed to –OH stretching vibration. Further, the bending vibrations of O-H were observed at 1647 cm^{-1} and 1642 cm^{-1} in control and treated sample respectively. The emergence of these vibrations could be due to water absorption by the sample. The control and treated samples showed the absorption band at 629 cm^{-1}, which was attributed to Sn-O stretching vibrations [30]. Furthermore, a band observed at 496 cm^{-1} in the control corresponding to Sn-OH vibration was shifted to 512 cm^{-1} [31]. The wavenumber ($\bar{\nu}$) indicated in IR spectra corresponding to the stretching vibration of a bond is directly related to the bond force constant (k) as following:

$$\bar{\nu} = \frac{1}{2\pi c}\sqrt{\frac{k}{\mu}}$$

Here, μ is the effective mass of atoms, which form the bond and c is the speed of light (3×10^8 m/s). Thus, the shifting of wavenumber corresponding to Sn-OH bond in treated sample indicated that the bond force constant of Sn-OH bond probably increased after the biofield energy treatment. Previously, our group reported that biofield energy treatment has altered the bond length of Ti-O bond in barium titanate [32]. Thus, it is possible that the energy transferred through biofield treatment probably acted on the atomic level to cause these modification in bonding properties.

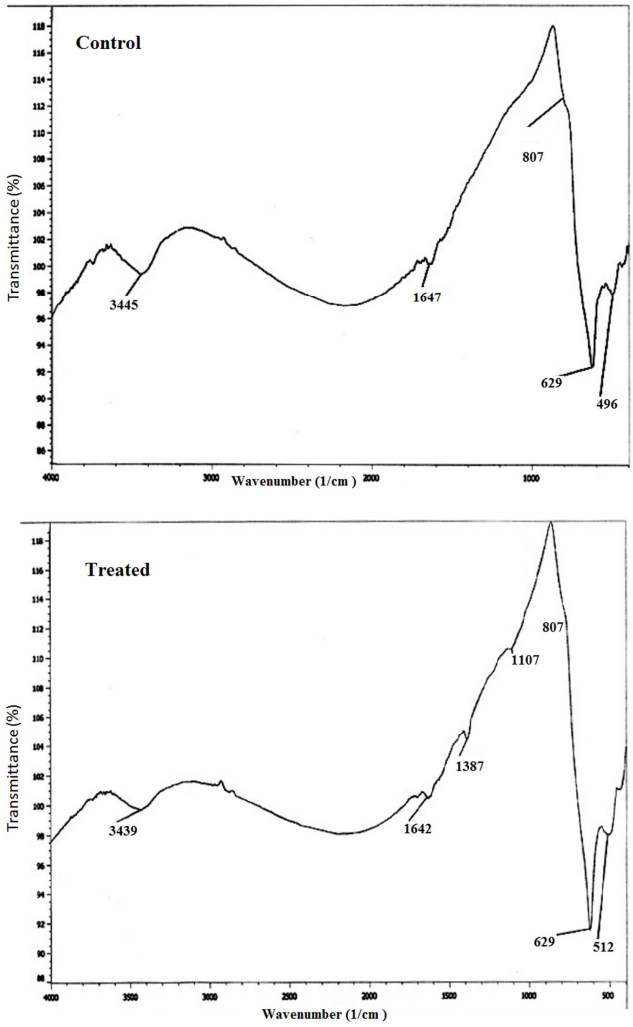

Fig. 2. *FT-IR spectra of antimony tin oxide nanopowder.*

3.3. ESR Spectroscopy

The EPR spectroscopy is extensively used to detect the presence of unpaired electrons and vacancies in the compounds. The ESR analysis result of control and treated ATO is presented in Table 3. The data showed that the g-factor of control ATO sample was found at 2.554, which was reduced to 2.008 in the treated sample after biofield energy treatment. It indicated that g-factor of treated ATO sample was reduced by 21.1 % as compared to the control. Further, in ATO, the metal atoms were in the form of Sb^{+5} and Sn^{+4}, which do not have unpaired electron. Due to this, the metal cations could not produce the ESR signal. Thus, oxygen vacancy should be the only producer for EPR signals in control and treated samples [33]. Furthermore, the reduction of g-factor in treated sample indicated that the biofield energy treatment probably altered the oxygen vacancies present in the ATO sample. Thus, the alterations in the oxygen vacancies in treated ATO sample may change its conductivity. Further, it was also found that the signal intensity of the ESR peak was reduced by 70.4% in the treated ATO sample as compared to the control. Moreover, the height of the ESR signal of the treated sample was reduced by 93.7% as compared to the control. Thus, above data indicated that biofield energy treatment might alter the positions of oxygen vacancies in the treated ATO sample, which resulted into alterations in width and height of the ESR signal.

Table 3. *ESR analysis result of antimony tin oxide nanopowder.*

Group	g-factor	ESR signal width	ESR signal height
Control	2.554	270	1.48×10^{-3}
Treated	2.008	80	9.38×10^{-5}
Percent Change	-21.1	-70.4	-93.7

4. Conclusions

The XRD data revealed that the crystallite size of the plane (110) was significantly reduced up to 53.1 nm in the treated ATO sample as compared to the control (212.6 nm). The decrease in crystallite size may lead to alter the conductivity of treated ATO sample. Furthermore, the FT-IR spectra showed that the stretching vibration peak corresponding to Sn-OH was shifted to higher wavenumber (512 cm^{-1}) as compared to the control (496 cm^{-1}). It could be due to the alteration in bonding properties of treated ATO sample after biofield energy treatment. Besides, the ESR spectra analysis exhibited that the g-factor was reduced in treated ATO sample by 21.1% as compared to the control. Also, the ESR signal width and height were reduced by 70.4% and 93.7%, respectively in treated sample as compared to the control. Hence, the XRD, FT-IR, and ESR data revealed that the biofield energy treatment has a significant impact on the atomic and physical properties of ATO nanopowder. Therefore, the biofield energy treatment could be used to modify the atomic and physical properties of ATO for display devices and solar cell applications.

Acknowledgments

Authors would like to acknowledge Dr. Cheng Dong of NLSC, Institute of Physics, and Chinese academy of sciences for supporting in analyzing the XRD data using Powder-X software. The authors would also like to thank Trivedi Science, Trivedi Master Wellness and Trivedi Testimonials for their support during the work.

References

[1] Babar AR, Shinde SS, Moholkar AV, Bhosale CH, Kim JH, et al. (2011) Physical properties of sprayed antimony doped tin oxide thin films: The role of thickness. J Semiconduct 32: 053001.

[2] Vaufrey D, Khalifa MB, Besland MP, Sandu CS, Blanchin MG, et al. (2002) Reactive ion etching of sol–gel-processed SnO_2 transparent conductive oxide as a new material for organic light emitting diodes. Synthetic Metals 127: 207-211.

[3] El-Etre AY, Reda SM (2010) Characterization of nanocrystalline SnO_2 thin film fabricated by electrodeposition method for dyesensitized solar cell application. Appl Surf Sci 256: 6601-6606.

[4] Chappel S, Zaba A (2002) Nanoporous SnO_2 electrodes for dyesensitized solar cells: improved cell performance by the synthesis of 18 nm SnO_2 colloids. Sol Energ Mat Sol Cells 71: 141-151.

[5] Fang C, Wang S, Wang Q, Liu J, Geng B (2010) Coralloid SnO_2 with hierarchical structure and their application as recoverable gas sensors for the detection of benzaldehyde/acetone. Mater Chem Phys 122: 30-34.

[6] Ming YH, Hua HY, Zhou QG (2002). Preparation of antimony-doped SnO_2 nanocrystallites, Mater Res Bull 37: 2453-2458.

[7] Li LL, Ming ML, Chen DX (2006) Solvothermal synthesis and characterization of Sb-doped SnO_2 nanoparticles used as transparent conductive films. Mater Res Bull 41: 541-546.

[8] Qin G, Li D, Chen Z, Hou Y, Feng Z, Liu S (2009) Structural, electronic and optical properties of $Sn_{1-x}SbxO_2$. Comp Mater Sci 46: 418-424.

[9] Rockenberger J, zum Felde U, Tischer M, Troger L, Haase M, et al. (2000) Near edge X-ray absorption fine structure measurements (XANES) and extended X-ray absorption fine structure measurements (EXAFS) of the valence state and coordination of antimony in doped nanocrystalline SnO_2. J Chem Phys 112: 4296.

[10] Stjerna B, Olsson E, Granqvist CG (1994) Optical and electrical properties of radio frequency sputtered tin oxide films doped with oxygen vacancies, F, Sb, or Mo. J Appl Phys 76: 3797-381.

[11] Krishnakumar T, Jayaprakash R, Pinna N, Phani AR, Passacantando M et al. (2009) Structural, optical and electrical characterization of antimony-substituted tin oxide nanoparticles. J Phys Chem Solids 70: 993-999.

[12] Zhang D, Deng Z, Zhang J, Chen L (2006) Microstructure and electrical properties of antimony-doped tin oxide thin film deposited by sol–gel process. Mater Chem Phys 98: 353-357.

[13] Zhang J, Gao L (2004) Synthesis of antimony-doped tin oxide (ATO) nanoparticles by the nitrate–citrate combustion method. Mater Res Bull 39: 2249-2255.

[14] Kersen U, Sundberg MR (2003) The reactive surface sites and the H_2S sensing potential for the SnO_2 produced by a mechanochemical milling. J Electrochem Soc 150: H129–H134.

[15] Willett J, Burganos MN, Tsakiroglou VD, Payatakes CC (1998) Gas sensing and structural properties of variously pretreated nanopowder tin (IV) oxide samples. Sensors and Actuat B: Chem 53: 76-90.

[16] Song KC, Kim JH (2000) Synthesis of high surface area tin oxide powders *via* water in-oil microemulsions. Powder Technol 107: 268-272.

[17] Saad M, Medeiros RD (2012) Distant healing by the supposed vital energy- scientific bases. Complementary therapies for the contemporary healthcare. InTech.

[18] Barnes PM, Powell-Griner E, McFann K, Nahin RL (2004) Complementary and alternative medicine use among adults: United States, 2002. Adv Data 343: 1-19.

[19] Trivedi MK, Nayak G, Patil S, Tallapragada RM, Latiyal O (2015) Studies of the atomic and crystalline characteristics of ceramic oxide nano nanopowders after bio field treatment. Ind Eng Manage 4: 161.

[20] Trivedi MK, Patil S, Nayak G, Jana S, Latiyal O (2015) Influence of biofield treatment on physical, structural and spectral properties of boron nitride. J Material Sci Eng 4: 181.

[21] Trivedi MK, Patil S, Shettigar H, Bairwa K, Jana S (2015) Phenotypic and biotypic characterization of *Klebsiella oxytoca*: An impact of biofield treatment. J Microb Biochem Technol 7:202-205.

[22] Trivedi MK, Nayak G, Patil S, Tallapragada RM, Latiyal O et al.(2015) An evaluation of biofield treatment on thermal, physical and structural properties of cadmium nanopowder. J Thermodyn Catal 6: 147.

[23] Trivedi MK, Tallapragada RM, Branton A, Trivedi D, Nayak G, et al. (2015) Potential impact of biofield treatment on atomic and physical characteristics of magnesium. Vitam Miner 3: 129.

[24] Trivedi MK, Patil S, Tallapragada RM (2013) Effect of biofield treatment on the physical and thermal characteristics of vanadium pentoxide nanopowder. J Material Sci Eng S11: 001.

[25] Thangaraju B (2002) Structural and electrical studies on highly conducting spray deposited fluorine and antimony doped SnO_2 thin films from $SnCl_2$ precursor. Thin Solid Films 402: 71-78.

[26] Ravichandran K, Philominathan P (2008) Fabrication of antimony doped tin oxide (ATO) films by an inexpensive, simplified spray technique using perfume atomizer. Mater Lett 62: 2980-2983.

[27] Kumar P, Kar M (2014) Effect of structural transition on magnetic and dielectric properties of La and Mn co-substituted $BiFeO_3$ ceramics. Mater Chem Phys. 148: 968-977.

[28] Singh R, Gupta S, Das B (2011) Synthesis and structural/microstructural characteristics of antimony doped tin oxide ($Sn_{1-x}Sb_xO_{2-\delta}$). Cond Mat Mtrl Sci. http://arxiv.org/pdf/1107.1807.pdf

[29] Zhang L, Wu J, Chena F, Li X, Schoenung JM (2013) Spark plasma sintering of antimony-doped tin oxide (ATO) nanoceramics with high density and enhanced electrical conductivity. J Asian Ceram Soc 1: 114-119.

[30] Morales FL, Zayas T, Contreras OE, Salgado L(2013) Effect of Sn precursor on the synthesis of SnO_2 and Sb-doped SnO_2 particles *via* polymeric precursor method. Front Mater Sci 7: 387-395.

[31] Xiaozhen L, Jie C, Yan W, Jie X (2009) Synthesis and characterization of Gd and Sb Doped SnO_2 conductive nanoparticles. Proceeding of ICNM – 2009 1st International Conference on Nanostructured Materials and Nanocomposites (6 – 8 April 2009, Kottayam, India).

[32] Trivedi MK, Nayak G, Patil S, Tallapragada RM, Latiyal O, et al. (2015) Impact of biofield treatment on atomic and structural characteristics of barium titanate nanopowder. Ind Eng Manage 4: 166.

[33] Cui Y, Feng Y (2005) EPR study on Sb doped Ti-base SnO_2 electrodes. J Mater Sci 40: 4695-4697.